Journal of ELECTRONIC MATERIALS, Vol. 38, No. 10, 2009
DOI: 10.1007/s11664-009-0883-3

*Regular Issue Paper*

# Rheological Behavior of Thermal Interface Pastes

CHUANGANG LIN[1] and D.D.L. CHUNG[1,2]

1.—Composite Materials Research Laboratory, University at Buffalo, State University of New York, Jarvis Hall, Room 318, Buffalo, NY 14260-4400, USA. 2.—e-mail: ddlchung@buffalo.edu

Polyol-ester-based thermal pastes containing carbon black, fumed alumina or nanoclay exhibit Bingham plastic behavior with shear thinning. Carbon black gives double yielding, but fumed alumina and nanoclay give single yielding. The plastic viscosity increases with the solid content. Antioxidants increase the plastic viscosity and yield stresses. Nanoclay (1.0 vol.%) gives low shear moduli, high critical shear strain, and high loss tangent, thus resulting in low bond-line thickness and high thermal contact conductance for smooth (0.009 $\mu$m) proximate surfaces. Carbon black (Tokai, 8.0 vol.%) gives high moduli, low critical strain, and low loss tangent, thus resulting in high bond-line thickness, though the high thermal conductivity due to the high solid content results in high thermal contact conductance for rough (15 $\mu$m) proximate surfaces. Antioxidants enhance the solid-like character, increase the yield stress, plastic viscosity, and bond-line thickness, and decrease the thermal contact conductance.

**Key words:** Thermal interface material, thermal paste, polyol ester, carbon black, fumed alumina, nanoclay, antioxidants, rheology, shear modulus, critical shear strain

## INTRODUCTION

Thermal interface materials (TIMs)[1–6] are commonly used to improve thermal contacts for the purpose of microelectronic cooling. The TIM is used to reduce the thermal contact resistance arising from the incomplete contact between two solid surfaces, which are never perfectly flat. TIMs are mainly in the form of pastes, which are known as thermal pastes.[5,6] Thermal pastes comprise thermally conducting solids, such as metals, ceramics, and carbon, which are incorporated in liquids that are typically various hydrocarbons or silicone oils.[7–9] Additionally, other ingredients such as antioxidants and/or phase stabilizers are often present in small amounts.[10]

Thermal conductivity has long been assumed in the TIM industry to be the key criterion in determining the effectiveness of a TIM. Conventional solid components include various metal and ceramic particles that exhibit high thermal conductivity. For maximizing the highest thermal conductivity, the degree of loading of the solid ingredients is conventionally maximized, as allowed by the geometric packing and the paste workability. The concentration of solids in a thermal paste typically exceeds 70 vol.%. However, an excessive solid content is detrimental to the workability, conformability, and spreadability of the paste, though it helps the thermal conductivity within the paste.[11]

Workability is necessary for the application of the paste to a surface by printing, which involves extrusion of the paste, the pushing of the paste through the holes of a screen, and related methods. Conformability allows the paste to displace air from the valleys in the topography of the proximate surfaces. Spreadability allows the paste to have a small thickness (ideally just enough to fill the valleys), which helps limit the thermal resistance. Due to the small size of the valleys, the nanostructuring of the paste helps both the conformability and the spreadability. Nanostructuring can be obtained by the use of solid components that are in the nanoscale. Nanoscale solid components that have been found to be effective to various degrees include

(Received April 2, 2009; accepted June 17, 2009; published online July 10, 2009)

carbon black (CB),[12–16] graphite nanoplatelet (GNP),[17,18] fumed metal oxides (e.g., fumed alumina),[19] and nanoclay.[20,21]

The rheological behavior refers to the flow behavior, which is basic to the behavior of any type of paste. This behavior pertains to the stress and strain associated with shear deformation of the paste at various strain rates and relates to the viscosity, yield stress, storage modulus, loss modulus, loss tangent, critical shear strain (strain at the limit of the linear regime in which stress and strain are linearly related), and their dependence on temperature and the formulation. The behavior governs the workability, conformability, and spreadability of the paste. Due to the elevated temperatures encountered by a thermal paste during use, information on the effect of temperature is of practical importance. Furthermore, the effect of the formulation provides valuable information for guiding the design of thermal pastes.

Prior work[16,18,20,22] on the rheology of thermal pastes has emphasized viscosity measurement, with relatively little attention being paid to the yield stress, storage modulus, loss modulus, loss tangent, and critical strain. This limitation stems from the fact that the rheological study in much of the prior work was measured by using a viscometer rather than a rheometer, which is powerful for dynamic rheological behavior study.

Prior work involving rheometry of thermal pastes[23,24] has addressed the viscosity, yield stress, storage modulus, loss modulus, and the effect of temperature on the viscosity and moduli, but pastes were limited to those with high solid volume fractions, namely 40 vol.% to 60 vol.% aluminum particles[23] and above 72 vol.% mixture of aluminum and alumina particles.[24] These particles are 7.9 $\mu$m spherical aluminum[23] and presumably not in the nanoscale also for Ref. 24. The rheology is expected to be quite different when the particles are in the nanoscale. In particular, the viscosity and the yield stress are expected to be higher when the particles are in the nanoscale. The present work addresses the rheometry of thermal pastes with low volume fractions (8 vol.% or below) of nanoscale solid components.

The prior work on the rheology of thermal pastes is limited to vehicles in the form of silicone oil[23] or an unspecified hydrocarbon oil.[24] The present work addresses the rheometry of thermal pastes with a polyol ester vehicle. This vehicle is widely used in state-of-the-art thermal pastes, due to its combination of fluidity and elevated temperature resistance.

Antioxidants that are dissolved in the vehicle are commonly used in commercial thermal pastes for the purpose of increasing the ability to withstand elevated temperature. This work investigates the effect of antioxidants on the rheology. Prior work[22] on the effect of antioxidants is limited to investigation using a viscometer, with no determination of the yield stress or shear moduli. This prior work also addresses the effect of prior heating on the viscosity. The present work provides the first investigation of the effect of temperature during heating on the viscosity of thermal pastes.

Prior work involving rheometry has involved carbon black (15 vol.%) aqueous dispersions,[25] which are not suitable for use as thermal pastes due to the volatility of water and the requirement for thermal pastes to withstand elevated temperatures. The double yielding behavior (i.e., the presence of two yield stresses) for the intermediate polymer content was observed in the prior work.[25] The second yielding, which occurs at a higher shear stress, was attributed in the prior work to the interaction of the polymer film on the carbon black with the polymer in the water. For lower or higher polymer contents, only single yielding was observed. No explanation is provided for the effect of the polymer content on the yielding phenomenon.

The objectives of this work are (i) to provide characterization of state-of-the-art nanostructured polyol-ester-based thermal pastes in terms of their rheology, including the storage and loss moduli, yield stress (or yield stresses in case of double yielding), loss tangent, plastic viscosity, apparent viscosity, and critical strain; (ii) to provide a comparative study of the rheology of thermal pastes with various solid components, including carbon black, fumed alumina, and nanoclay; and (iii) to investigate the effect of antioxidants on the rheology, and its temperature dependence.

## BACKGROUND ON RHEOLOGY

The complex shear modulus $G$ is given by

$$G = \tau/\gamma, \tag{1}$$

where

$$\tau = \tau_o e^{i\omega t} \tag{2}$$

is the shear stress, with $\tau_o$ being the amplitude of the shear stress wave and $\omega$ being the angular frequency, and

$$\gamma = \gamma_o\ e^{i(\omega t - \delta)} \tag{3}$$

is the shear strain, with $\gamma_o$ being the amplitude of the shear strain wave and $\delta$ being the lag (phase) angle, in radians. Hence,

$$G = (\tau_o/\gamma_o)e^{i\delta} = (\tau_o/\gamma_o)(\cos\,\delta + i\sin\,\delta), \tag{4}$$

and

$$\begin{aligned}\tan\delta &= (\sin\delta)/(\cos\delta)\\ &= (\text{imaginary part of } G)/(\text{real part of } G).\end{aligned} \tag{5}$$

The real part of $G$ (abbreviated as $G'$) is called the storage modulus, which describes the elastic

behavior. The imaginary part of $G$ (abbreviated as $G''$) is called the loss modulus, which describes the viscous behavior. The quantity $\tan\delta$ is called the loss tangent. Hence,

$$G = G' + iG'', \tag{6}$$

where

$$G' = (\tau_o/\gamma_o)\cos\delta, \tag{7}$$

and

$$G'' = (\tau_o/\gamma_o)\sin\delta. \tag{8}$$

The magnitude of $G$, which is a complex quantity, is given by

$$|G| = \tau_o/\gamma_o. \tag{9}$$

Equation 5 can be rewritten as

$$\tan\delta = G''/G'. \tag{10}$$

For a particle paste, the strength of the colloidal forces between the particles is reflected by $\tan\delta$. A $\tan\delta$ value less than 1 suggests that the particles are highly associated due to the colloidal forces and sedimentation could occur. In contrast, a value of $\tan\delta$ exceeding 1 suggests that the particles are largely unassociated. The smaller $\tan\delta$, the stronger the interaction of the particles.

The frequency relates to the strain rate, as shown by differentiating Eq. 3:

$$\dot{\gamma} = \gamma_o i\omega\, e^{i(\omega t-\delta)}. \tag{11}$$

This means that a higher $\omega$ is associated with a higher strain rate.

Applying a constant strain below the critical value and an angular frequency ramp reveals the microstructure of a material through the response of the material to different shear rates. Under an oscillatory strain, stress relaxation may occur. As $\omega$ increases, a certain relaxation mechanism in the material may start to be unable to operate fast enough. A smaller degree of stress relaxation results in a higher stress and hence higher values of $G'$ and $G''$. As a result, $G'$ and $G''$ increase with increasing $\omega$. As both stress relaxation and viscous deformation are time-dependent processes, this effect of $\omega$ on $G''$ tends to be larger than that on $G'$. As a result, $\tan\delta$ tends to be increased. On the other hand, as $\omega$ increases, the viscous deformation may not have enough time to occur to its fullest, thus causing $\delta$ (and hence $\tan\delta$) to be effectively smaller, making $G''$ lower and $G'$ higher.

The critical shear strain $\gamma_c$ is the strain at the limit of linear behavior (i.e., characterized by the linear relationship between shear stress and shear strain), so that $G'$ and $G''$ are independent of the strain. Above $\gamma_c$, linear behavior is lost due to the loss of a certain type of structure in the material.

The shear yield stress $\tau_y$ is defined as the minimum shear stress required to initiate shear flow. The viscosity $\eta$ is defined as

$$\tau = \eta\dot{\gamma}. \tag{12}$$

For a Newtonian fluid, there is no yielding (i.e., no yield stress), so the shear strain rate (also called the shear rate) $\dot{\gamma}$ is constant at a constant stress $\tau$, and hence $\eta$ is independent of the shear strain rate. For a non-Newtonian material, $\eta$ varies with the shear strain rate. If $\eta$ decreases with increasing shear rate, the behavior is said to be shear thinning.

In general, a particle paste behaves as a Bingham plastic, so that it exhibits yielding and the viscosity is described as the plastic viscosity, which is the slope of the plot of the shear stress $\tau$ versus the shear strain rate $\dot{\gamma}$ above the yield stress $\tau_y$. The widely used two-parameter Bingham plastic model is described by the equation

$$\tau = \tau_y + \eta_p\dot{\gamma}, \tag{13}$$

where $\tau_y$ is the yield stress and $\eta_p$ is the plastic viscosity. In the case of shear thinning or thickening, the slope is not constant and the plastic viscosity is thus not constant.

The plastic viscosity is to be distinguished from the apparent viscosity, which is given by the shear stress divided by the corresponding shear rate at a particular shear rate and is a parameter provided directly by a rheometer during testing. For a Bingham plastic, the apparent viscosity differs from the plastic viscosity, which is more meaningful scientifically.

From Eqs. 2, 9, 11, and 12,

$$\eta = \tau_o e^{i\omega t}/\left[\gamma_o i\omega\, e^{i(\omega t-\delta)}\right] = -i(|G|/\omega)e^{i\delta}. \tag{14}$$

The magnitude of $\eta$ is thus given by

$$|\eta| = |G|/\omega. \tag{15}$$

Equation 15 means that $|\eta|$ is inversely related to $\omega$.

## EXPERIMENTAL PROCEDURES

### Materials

All the thermal pastes studied use the same vehicle, namely polyol esters, as used in prior work.[16,18–20,22] The polyol esters in the vehicle are (i) pentaerythritol ester of linear and branched fatty acids and (ii) dipentaerythritol ester of linear and branched fatty acids. The polyol ester mixture is Hatcol 2372, as provided by Hatco Corp., Fords, NJ. /Para>A combination of primary antioxidant (SUMILIZER GA-80, Sumitomo Chemical Corp., at 0.500 wt.% of the vehicle) and secondary antioxidant (SUMILIZER TP-D, Sumitomo Chemical

Corp., at 1.000 wt.% of the vehicle) dissolved in the vehicle is used to promote the thermal stability of the pastes. Detailed information on the selected antioxidants is given in prior work.[22] Both the cases with and without antioxidants are included in the present study.The solid components used in the thermal pastes are carbon black (CB, including two types that differ in the aggregate size, as indicated by the DBP values[16]; the type of larger aggregate size being Vulcan XC72R GP-3820, Cabot Corp., Billerica, MA, and the type with smaller aggregate size being Tokaiblack #3800, a graphitized carbon black supplied by Tokai Carbon Co., Ltd., Tokyo, Japan), trimethoxyoctylsilane-treated fumed alumina (Aeroxide ALU C 805, Degussa AG, Hanau, Germany[19]), and nanoclay (Cloisite 15A, Southern Clay Products, Inc., Gonzales, TX; a natural montmorillonite phyllosilicate intercalated with an organic modifier, namely dimethyl dehydrogenated tallow, a quaternary ammonium salt at 125 meq/100 g clay[20]). The compositions of the various pastes and the particle sizes of the fillers are listed in Table I.

### Rheological Testing

The rheological properties of various thermal pastes were measured using an AR G2 rheometer (TA Instruments, New Castle, DE). All experiments used 40-mm-diameter circular aluminum disks in a parallel-plate configuration. In this configuration, the proximate surfaces of the two plates are separated by a fixed gap (1000 ± 1 $\mu$m) that is filled with the paste under study. The top plate rotates while the bottom plate is stationary, thus providing torsional deformation of the paste under study. The paste under study is located only in the space between the two plates. Experiments are conducted under both continuous (steady-state) shear and oscillatory (dynamic) shear. The temperature is 25°C, unless noted otherwise. Steady-state shear torque ramp is conducted by increasing the torque from 1 $\mu$N m to 2000 $\mu$N m. This corresponds to the shear stress increasing from 0.8 Pa to 158 Pa and gives rise to increase of the shear strain rate. However, in some tests, the shear stress increases from 0.5 Pa to 50 Pa. The dynamic strain sweep tests are conducted for strain ranging either from 0.01% to 10% or from 0.01% to 100%, all at an angular frequency of 6.28 rad/s (i.e., a frequency of 1 Hz). Dynamic frequency sweep is conducted in an angular frequency range of 0.1 rad/s to 100 rad/s at a constant strain amplitude (also referred to as a constant strain) in the linear regime, the limit of which is determined by strain sweep (an increase in the strain amplitude by small discrete steps). The value of the constant strain amplitude differs among the types of specimens, which differ in the critical strain. For example, for the vehicle with antioxidants but without a solid component, the constant strain amplitude is 10%; for the CB(Cabot) paste with antioxidants, the constant strain amplitude is 0.2%. Dynamic temperature ramping is conducted by increasing the temperature from 25°C to 120°C at a heating rate of 3°C/min and a frequency of 1 Hz within the linear regime.

## RESULTS AND DISCUSSION

### Critical Strain Determined by Strain Sweep

For the purpose of studying the linear regime of the deformation, the critical strain $\gamma_c$ needs to be determined.[26] Thus, the amplitude of the dynamic (oscillatory) strain is swept, while $G'$ is measured. In this study, $\gamma_c$ is taken as the strain at which $G'$ has decreased by 5%. To save space herein, only the strain sweep curve of the CB(Cabot) paste is shown in Fig. 1. However, the values of $G'$, $G''$, critical strain, and tan $\delta$ obtained from the results for the various types of paste are summarized in Table II.

Figure 1 shows that, for the CB(Cabot) paste, $\gamma_c$ is about 1.5%. Below a strain of 1.5%, the paste behaves like a solid, with $G' > G''$, indicating that the material is highly structured, probably like a network. Above $\gamma_c$, the structure is disrupted and the paste becomes more and more like a fluid,[27–29] with both $G'$ and $G''$ deceasing with increasing

**Table I. Compositions of the Thermal Pastes Studied**

| Vehicle | Solid Component | Particle Size | Solid Component, vol.% |
|---|---|---|---|
| Vehicle without A | – | – | – |
| Vehicle with A | – | – | – |
| Vehicle without A | Nanoclay | 1 nm thick, 70 nm to 150 nm across (after exfoliation)[20] | 1.0 |
| Vehicle without A | Fumed alumina | 13 nm | 2.4 |
| Vehicle without A | Carbon black (Cabot) | 30 nm | 2.4 |
| Vehicle with A | Carbon black (Cabot) | 30 nm | 2.4 |
| Vehicle without A | Carbon black (Tokai) | 70 nm | 8.0 |

A = antioxidants.

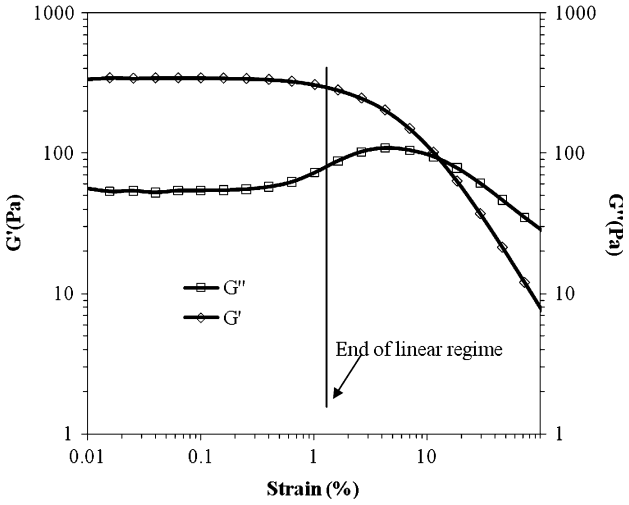


Fig. 1. Strain sweep for CB(Cabot) thermal paste, showing $G'$ and $G''$ in the linear regime and beyond.

**Table II. Strain Sweep Results of Thermal Pastes, Showing the Values of $G'$, $G''$, and tan $\delta$ Below the Critical Strain $\gamma_c$ at Angular Frequency of 6.28 rad/s**

| Paste | $G'$ (Pa) | $G''$ (Pa) | $\gamma_c$ (%) | tan $\delta$ |
|---|---|---|---|---|
| Nanoclay | 25 | 15 | 10.0 | 0.60 |
| Fumed alumina | 45 | 20 | 1.5 | 0.56 |
| CB(Cabot) | 350 | 55 | 1.5 | 0.16 |
| CB(Cabot) + A | 840 | 88 | 0.5 | 0.11 |
| CB(Tokai) | 6,500 | 650 | 0.1 | 0.10 |
| Ref. 24 | $\sim 4.2 \times 10^5$ | $\sim 2 \times 10^5$ | 0.1 | $\sim$0.48 |

A = antioxidants.

strain and $G''$ exceeding $G'$ when the strain exceeds 10%. Similar behavior occurs for all of the other pastes, as shown in Table II and discussed below.

The critical strain, which relates to the minimum energy needed to disrupt the structure, depends on the dispersion quality. The higher the critical strain, the better the degree of dispersion.[27,30] Table II shows that the nanoclay paste has the highest critical strain, i.e., the highest degree of dispersion. The value is much higher than those of the other pastes. This is believed to be due to the organic modification of the nanoclay, which makes the clay surface highly hydrophobic and hence compatible with the polyol ester vehicle, which is commercially available as a lubricant oil. The high degree of dispersion of the nanoclay is consistent with the value of tan $\delta$, which is higher than that of any of the other pastes studied (Table II). In general, the higher tan $\delta$, the more the paste is like a fluid and the lower the tendency for phase separation.

In Table II, the CB(Tokai) paste has the lowest critical strain, i.e., the lowest degree of dispersion.[30] Two reasons may be behind the low degree of dispersion for the CB(Tokai) paste. Firstly, the CB(Tokai) has been graphitized, and the graphitization heat treatment may reduce the hydrophobicity of the carbon black. Secondly, the volume fraction of the solid component is much higher for the CB(Tokai) paste than the other pastes in Table II, thus making the paste more like a solid (as shown by a low value of tan $\delta$) and causing the dispersion of the solid component to be more difficult.

Upon addition of the antioxidants, the critical strain of the CB(Cabot) paste decreases from 1.5% to 0.5% and tan $\delta$ decreases from 0.16 to 0.11 (Table II). This means that the degree of dispersion of carbon black is decreased by the addition of antioxidants and that the antioxidants cause the paste to be more like a solid.

The CB(Cabot) paste and the fumed alumina paste are similar in solid component volume fraction and in $\gamma_c$, but tan $\delta$ is much higher for the latter. This means that the CB(Cabot) paste is more like a solid than is the fumed alumina paste, though the degree of dispersion is similar for the two pastes. This difference is probably due to the silane coating on the fumed alumina, although it may also be due to differences in the specific surface area and density between CB(Cabot) and fumed alumina.

Table II shows that $G'$ exceeds $G''$ for all the pastes studied, indicating that all the pastes are more like solids than fluids below the critical strain. Both parameters vary greatly among the various pastes, though the variation of $G'$ is more significant than that of $G''$. The value of $G'$ is particularly high for the CB(Tokai) paste, due to the high solid component volume fraction of this paste. The value of $G'$ is particularly low for the nanoclay paste, due to the low solid component volume fraction and the high degree of dispersion of the solid component.

The thermal pastes in the form of a hydrocarbon oil filled with a mixture of alumina and aluminum particles, as reported by Feger et al.,[24] show $G'$ and $G''$ values as high as $10^5$ Pa, which is much higher than those of any of the thermal pastes addressed here (Table II). This is probably because the pastes of Feger et al. are highly filled with solid components (>72 vol.%). Though the tan $\delta$ value is not reported by Feger et al.,[24] it can be estimated from the reported curve to be about 0.48, which is less than that of the nanoclay paste and the fumed alumina paste of this work. The paste of Feger et al. shows a critical strain of 0.1%, which is similar to that of the CB(Tokai) paste of this work.

## Plastic Viscosity and Shear Yield Stress Determined by Shear Stress Sweep

A steady-state shear torque ramp test is conducted in order to obtain information on the flow behavior, such as the yield stress, the plastic viscosity, and the extent of shear thinning. It should be noted that, before yielding, the specimen does not

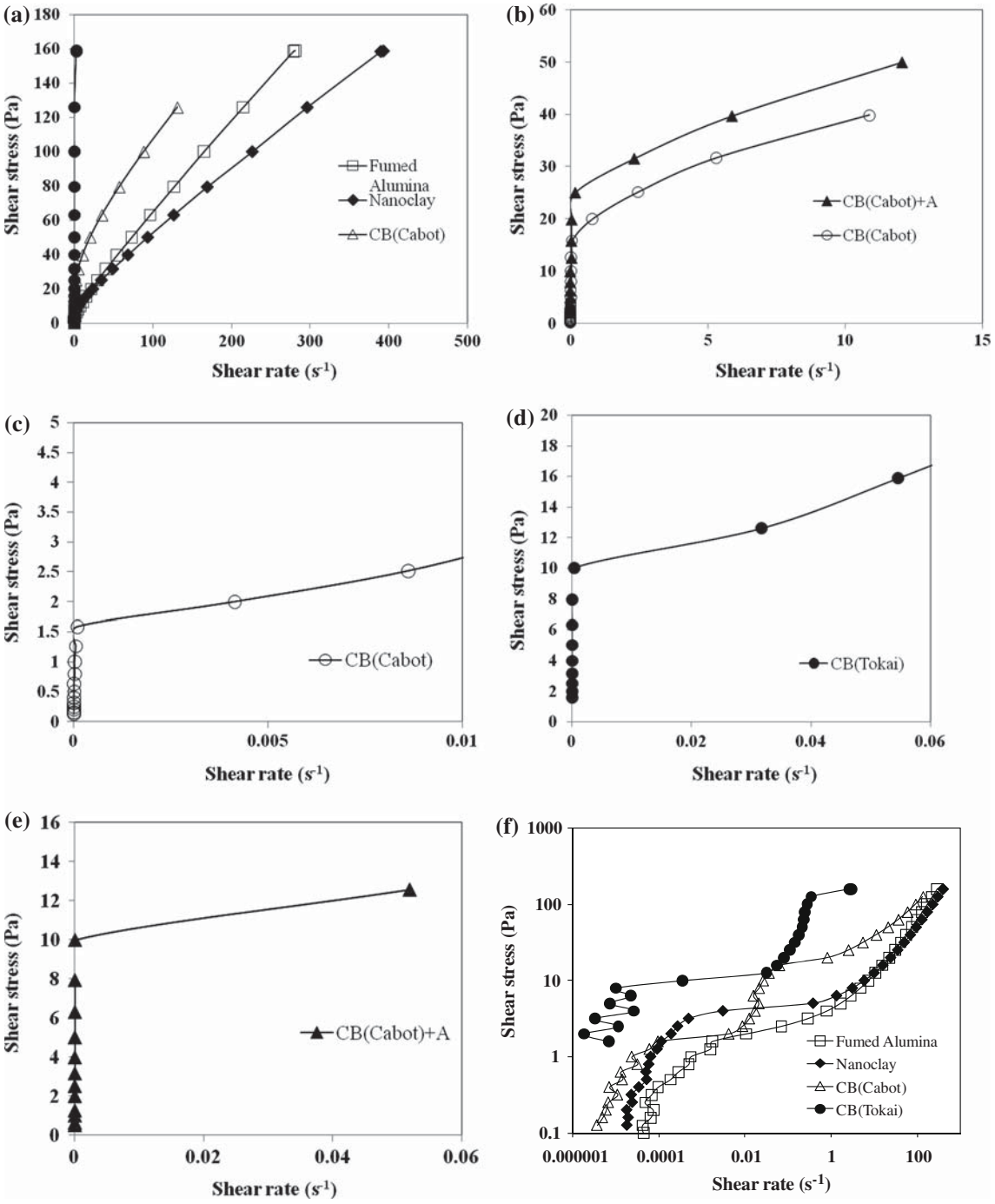


Fig. 2. Shear stress versus shear rate, showing the effect of the applied shear stress on the shear strain rate for various thermal pastes on a linear (a–e) and log (f) scale. The part of the curve immediately after the first yielding is magnified in (c–e). In (a) and (b), only the second yielding can be discerned, due to the small values of the first yield stress. A = antioxidants.

really flow and the shear rate is thus very small. Therefore, it is difficult to measure the shear rate or the apparent viscosity accurately before yielding. In this situation, the data scatter of the measured apparent viscosity is high. Figure 2 shows the relationship between shear stress (controlled during testing) and shear strain rate (also called the shear rate) for various thermal pastes. All the pastes are Bingham plastics, with the occurrence of yielding at a certain yield stress prior to flow.[31] For the vehicle in the absence of a solid component, there is no yielding. The vehicle itself is Newtonian, at least when antioxidants are absent.

Figure 2 shows the effect of increasing shear stress on the shear rate. Figure 2a shows the results for the entire range of shear stress studied. Bingham plastic behavior occurs for all of the pastes.[31] In other words, yielding, which is indicated

**Table III. Shear Yield Stress, as Measured by Steady-State Flow at Various Shear Stresses**

| | First Yield Stress (Pa) | Second Yield Stress (Pa) |
|---|---|---|
| Nanoclay | 4.2 | – |
| Fumed alumina | 2.9 | – |
| CB(Cabot) | 1.6 | 16.2 |
| CB(Tokai) | 7.7 | 160[a] |
| CB(Cabot) + A | 10[a] | 25.0 |

A = antioxidants. [a]Value is not reliable, due to the limited number of data points after yielding.

by a decrease in slope of the plot of shear stress versus shear rate, occurs, as more clearly shown in the magnified views in the low-stress regime in Fig. 2b–e. For the CB pastes, double yielding occurs, i.e., two yield stresses are present; the first yielding is shown in Fig. 2c–e. Due to the large difference in shear stress or shear rate between the two yield stresses, only the second yielding is shown in the linear-linear plots in Fig. 2a and b. However, in the log–log plot in Fig. 2f, the double yielding is clear. For the nanoclay paste and the fumed alumina paste, only single yielding occurs (Fig. 2a, f).

Among the fumed alumina, nanoclay, CB(Cabot), and CB(Tokai) pastes, all without antioxidants, the nanoclay paste gives the highest strain rate for the same shear stress, and the CB(Tokai) paste gives the lowest shear rate for the same shear stress (Fig. 2a). The low ability of the CB(Tokai) paste to flow is attributed to the high volume fraction (8%) of the solid component. The high ability for the nanoclay paste to flow is attributed to the low solid volume fraction (1%). Although the fumed alumina paste and the CB(Cabot) paste have the same solid volume fraction (2.4%), the ability to flow is greater for the former. The relatively high flow ability of the fumed alumina paste is probably partly due to the silane coating on the fumed alumina and the low specific surface area compared with CB(Cabot).[19] Figure 2b shows that the ability to flow is diminished by the presence of antioxidants.

The slope of the part of the curve above the yield stress is the plastic viscosity.[31] The yield stresses are listed in Table III. As yielding is also accompanied by an abrupt drop in the apparent viscosity, the single yielding behavior of the nanoclay paste and the fumed alumina pastes, and the double yielding behavior of the carbon black pastes, are further shown in Figs. 3, 4, and 5 as plots of apparent viscosity versus shear rate. The yield stresses indicated by the plots of shear stress versus shear rate and listed in Table III are consistent with those indicated by the plots of apparent viscosity versus shear rate.

The yielding occurs in two steps (i.e., double yielding) for the CB pastes, but occurs in one step

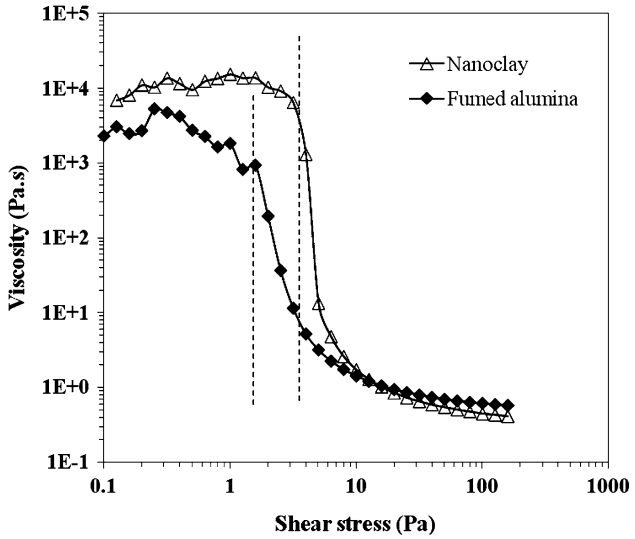


Fig. 3. Apparent viscosity versus shear stress for the nanoclay paste and the fumed alumina paste. The abrupt drop in apparent viscosity occurs at the shear yield stress.

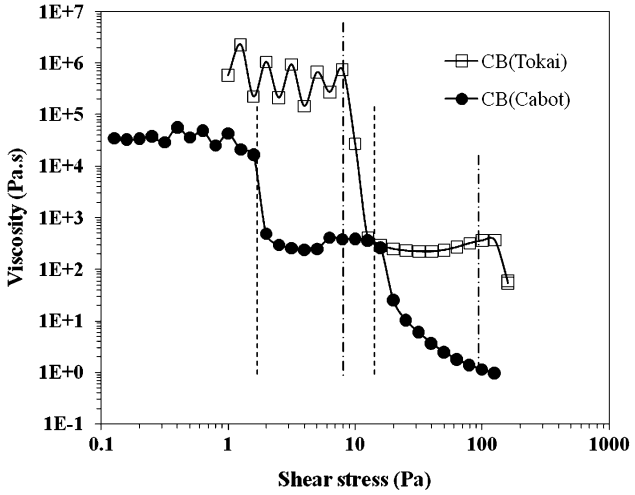


Fig. 4. Apparent viscosity versus shear stress for the CB(Tokai) paste and the CB(Cabot) paste. The abrupt drops in viscosity occur at the shear yield stresses. There are two yield stresses for each paste.

(i.e., single yielding) for the nanoclay and fumed alumina pastes. Figure 2a and Table IV show that the plastic viscosity after second yielding and subsequent shear thinning is lowest for the nanoclay paste (0.34 Pa s), followed by the fumed alumina paste (0.50 Pa s), then the CB(Cabot) paste (0.63 Pa s), then the CB(Tokai) paste (1 Pa s), and finally the CB(Cabot) paste with antioxidants (1.87 Pa s). This trend among the pastes is consistent with the lowest solid volume fraction in the nanoclay paste, the higher solid volume fraction for the alumina and CB(Cabot) pastes, and the still higher solid volume fraction for the CB(Tokai) paste. The highest plastic viscosity for the CB(Cabot)

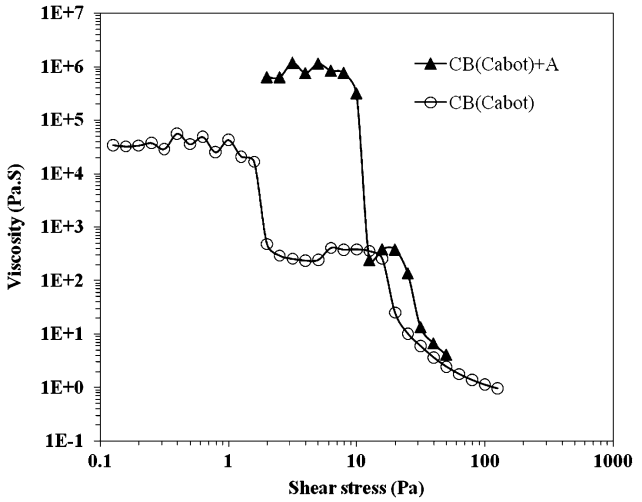


Fig. 5. Apparent viscosity versus shear stress for the CB(Cabot) paste with and without antioxidants. The abrupt drops in viscosity occur at the shear yield stresses. There are two yield stresses for each paste. A = antioxidants.

paste with antioxidants shows the significant increase of the viscosity due to the antioxidants. The fumed alumina paste has lower plastic viscosity than the CB(Cabot) paste, in spite of the identical solid volume fractions of these two pastes. This is probably because the fumed alumina has been silane treated.[19]

The plastic viscosity after second yielding is much lower than the corresponding value after first yielding. The plastic viscosity after first yielding is much higher for the CB pastes than for the nanoclay or fumed alumina paste. This means that the completion of yielding is not accomplished after the first yielding.

As shown in Table III, the second yield stress is much higher than the corresponding first yield stress. Among the various pastes, the CB(Cabot) paste has the lowest first yield stress, whereas the CB(Cabot) paste with antioxidants has the highest first yield stress. The CB(Tokai) paste gives the highest second yield stress. Both first and second yield stresses are much higher for the CB(Tokai) paste than the corresponding values of the CB(Cabot) paste. This is consistent with the higher solid component volume fraction (Table I) and higher $G'$ value (Table II) for the CB(Tokai) paste. Both the first and second yield stresses of the CB(Cabot) paste are increased by the addition of antioxidants. The fractional increase in the first yield stress due to the antioxidants is much higher than that of the second yield stress.

The first yield stress of the nanoclay paste is higher than those of the fumed alumina paste and the CB(Cabot) paste, although the volume fraction of the clay is the lowest among these pastes. This is believed to be due to the small particle size and the high aspect ratio of the exfoliated clay, since a smaller particle size and a higher aspect ratio are expected to give a higher yield stress.[20,32] This is consistent with the higher value of the critical strain for the nanoclay paste than for the other two pastes (Table II). The first yield stress of the nanoclay paste is smaller than that of the CB(Tokai) paste and that of the CB(Cabot) paste containing antioxidants. This is consistent with the high $G'$ values of the CB(Tokai) paste and the CB(Cabot) paste with antioxidants.

The occurrence of double yielding in the CB pastes is consistent with a prior report on an aqueous carbon black dispersion containing an appropriate concentration of polymer dissolved in the water.[25] The double yielding in the CB pastes is probably related to the aggregate structure of the carbon black. The first yielding may be due to the shear of one aggregate relative to another, whereas the second yielding may be due to the shear of one particle relative to another. Double yielding does not occur for the fumed alumina paste, in spite of the similar aggregate structure of fumed alumina, probably because of the partially polar nature of the bonding in alumina and the consequent greater cohesion among the alumina particles in an aggregate.

The first and second yield stresses are higher for the CB(Tokai) paste than those of any of the other pastes. This is attributed to the high solid volume fraction in the CB(Tokai) paste, as a higher filler volume fraction gives a higher yield stress in a filled polymer system.[32,33] The addition of antioxidants increases both the first and second yield stresses, as shown for the CB(Cabot) paste. This is probably because of the interaction of the antioxidants with the CB aggregate surface, making it more difficult for the aggregates to move relative to one another.

The yield stresses shown in Table III do not show correlation with the plastic viscosity shown in Table IV. Yielding is associated with the stress for the start of flow, and this stress depends on the structure before yielding. However, the plastic viscosity is associated with the ease of flow after flow initiation and it does not depend on the structure before yielding.

Figure 4 shows that the apparent viscosity below the first yield stress is higher for the CB(Tokai) paste than for the CB(Cabot) paste, but the apparent viscosity between the first and second yield stresses is similar for the two pastes. This means that the first yielding results in the same viscosity for the two pastes, even though the two pastes have different viscosity before the first yielding. This observation suggests that the viscosity associated with the movement of one aggregate relative to another is independent of the aggregate size. The viscosity before the first yielding is associated with macroscopic shear of the overall paste and is higher for the CB(Tokai) paste than for the CB(Cabot) paste, due to the higher solid component volume fraction in the CB(Tokai) paste.

Based on the apparent viscosity, the yield stress of aluminum-filled silicone was reported by

**Table IV. Decrease of the Plastic Viscosity with Increasing Shear Rate due to Shear Thinning**

| | Range of Shear Rate | | |
|---|---|---|---|
| | Start of Range ($s^{-1}$) | End of Range ($s^{-1}$) | Plastic Viscosity (Pa s) |
| Nanoclay | $3.07 \times 10^{-3}$[a] | 1.33 | 1.69 |
| | 3.09 | 9.90 | 0.68 |
| | 15.71 | 34.74 | 0.47 |
| | 49.04 | 93.41 | 0.37 |
| | 295.9 | 392.6 | 0.34 |
| Fumed alumina | 0.28[a] | 1.60 | 1.39 |
| | 2.83 | 7.09 | 0.86 |
| | 10.52 | 21.45 | 0.67 |
| | 29.62 | 54.44 | 0.59 |
| | 72.98 | 126.7 | 0.54 |
| | 215 | 278.6 | 0.50 |
| CB(Cabot) | $9.53 \times 10^{-5}$[a] | $8.61 \times 10^{-3}$ | 109.1 |
| | $1.24 \times 10^{-2}$ | $2.06 \times 10^{-2}$ | 226.22 |
| | $1.55 \times 10^{-2}$ | $2.61 \times 10^{-2}$ | 349.52 |
| | $6.17 \times 10^{-2}$[b] | 2.47 | 3.73 |
| | 10.88 | 35.31 | 0.95 |
| | 57.34 | 131.3 | 0.63 |
| CB(Tokai) | $3.66 \times 10^{-4}$[a] | $5.46 \times 10^{-2}$ | 106.6 |
| | $8.09 \times 10^{-2}$ | $1.42 \times 10^{-1}$ | 191.51 |
| | 2.66[b] | 2.99 | 1[c] |
| CB(Cabot) + A | $3.16 \times 10^{-5}$[a] | $4.1 \times 10^{-2}$ | 50[c] |
| | 0.18[b] | 5.88 | 2.54 |
| | 2.33 | 12.07 | 1.87 |

A = antioxidants. [a]Shear rate immediately after first yielding. [b]Shear rate immediately after second yielding. [c]Value is not reliable, due to the limited number of data points after yielding.

Prasher et al.[23] to be about 1.8 Pa for 40 vol.%, 9.9 Pa for 50 vol.%, and 55 Pa for 60 vol.% solid content. These values are in the range of the yield stress for the pastes of this work. The value of 4.2 Pa for the nanoclay paste of this work is substantial for the low nanoclay volume fraction of only 1.0% (much lower than the aluminum volume fractions of 40% or more in Ref. 23). The substantial value of the yield stress for the nanoclay paste is attributed to the nanoplatelet morphology, high aspect ratio, and large specific surface area of nanoclay and the consequent strong structure (network) even at low volume fraction.[34] Only single yielding was reported by Prasher et al.[23] and Feger et al.[24]

It should be noted that all the yield stresses are much smaller than the pressures (up to 1 MPa) used in measuring the thermal contact conductance of the thermal pastes between two proximate surfaces.

Figure 6 and Table V show the apparent viscosity versus the shear strain rate measured by steady-state shear using the torque ramp method. In other words, the increasing shear stress is controlled, while the apparent viscosity and the shear rate are measured. The effect on the shear rate is shown in Fig. 2, while the effect on the apparent viscosity is

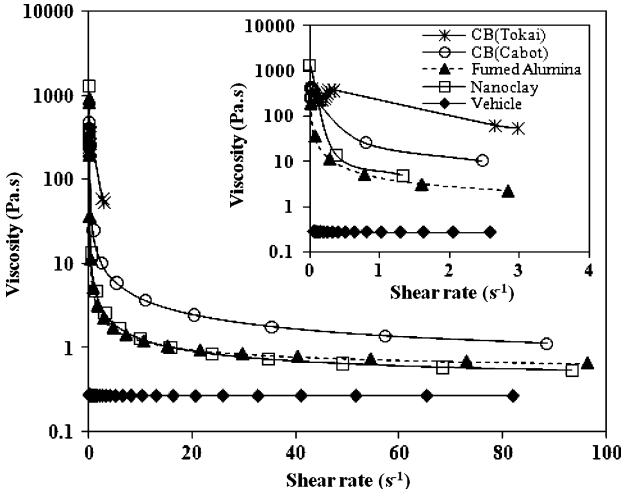


Fig. 6. Apparent viscosity (on logarithmic scale) versus shear strain rate for various thermal pastes. The inset shows a magnified view of the low strain rate region.

shown in Fig. 3. The vehicle without antioxidants or solid component is Newtonian, with the apparent viscosity not varying with the shear strain rate (Fig. 6). The apparent viscosity of the vehicle (by itself) is slightly different from that obtained in prior work by this group using a viscometer. The prior work shows slight shear-thinning behavior in the regime of low shear rate.[19] The apparent viscosity value is also different. For example, the apparent viscosity obtained by using a viscometer is 3650 cP (3.65 Pa s) at a shear rate of 0.127 $s^{-1}$,[19] but the apparent viscosity obtained in this work by using a rheometer is 0.274 Pa s at an almost identical shear rate of 0.129 $s^{-1}$. The discrepancy is probably due to the small value of the apparent viscosity of the vehicle.

In contrast, all the pastes (containing any of the solid components) are non-Newtonian, with shear-thinning behavior, i.e., the apparent viscosity decreasing with increasing shear rate. This is consistent with the decrease of the plastic viscosity with increasing shear rate (Table IV). The shear-thinning behavior has been previously reported for thermal pastes[16,19,20,22–24] and is common among filled polymer systems.[34]

The apparent viscosity is increased by the presence of any of the solid components, as shown in Fig. 3 and Table V. Among the various pastes, at the same shear rate, the apparent viscosity is highest for the CB(Tokai) paste, due to its high solid component volume fraction. It is lower for the CB(Cabot) paste and even lower for the fumed alumina paste and the nanoclay paste. That the apparent viscosity is lower for the fumed alumina paste than for the CB(Cabot) paste is consistent with the higher value of tan $\delta$ for the fumed alumina paste (Table II). That the apparent viscosities of the fumed alumina paste and the nanoclay paste are similar (Fig. 3) is consistent with the similarity of the tan $\delta$ values of these pastes (Table II).

**Table V. Apparent Viscosity of Thermal Pastes at Various Shear Rates (0 $s^{-1}$, 0.2 $s^{-1}$, and 0.4 $s^{-1}$)**

| Thermal Pastes | Apparent Viscosity (Pa s) | | |
|---|---|---|---|
| | 0 $s^{-1}$ | 0.2 $s^{-1}$ | 0.4 $s^{-1}$ |
| Fumed alumina | $1.60 \times 10^3$ | 15 | 8.5 |
| Nanoclay | $6.94 \times 10^3$ | 50 | 12.5 |
| CB(Cabot) | $3.43 \times 10^4$ | 150 | 68 |
| CB(Tokai) | $5.85 \times 10^5$ | 222 | 350 |
| CB(Cabot) + A | $1.15 \times 10^5$ | 145 | 102 |
| Vehicle | 0.28 | 0.27 | 0.27 |

A = Antioxidants.

Figure 6 and Table V show that the apparent viscosity drops sharply with increasing shear strain rate from 0 $s^{-1}$ to 0.4 $s^{-1}$ for all of the thermal pastes studied. This is consistent with prior work based on testing using a viscometer.[16,19,20]

## Effect of Frequency on the Apparent Viscosity and the Shear Moduli

Figure 7 shows the effect of $\omega$ on $G'$, $G''$, and $|\eta|$ (apparent viscosity) for various thermal pastes. For all the pastes, $|\eta|$ decreases with increasing $\omega$, as expected from Eq. 15.

For the nanoclay paste (Fig. 7a), $G'$ and $G''$ increase with increasing $\omega$, such that the increase is much more significant for $G''$ than for $G'$. This is probably due to the lessening stress relaxation as $\omega$ increases. At $\omega$ above 10 rad/s, $G''$ exceeds $G'$; at $\omega$ below 10 rad/s, $G'$ exceeds $G''$. This means that the paste becomes more and more like a fluid as $\omega$ increases, such that the fluid-like character dominates over the solid-like character when $\omega$ exceeds 10 rad/s.[27,29]

For the fumed alumina paste (Fig. 7b), $G''$ increases with increasing $\omega$, although not as significantly as for the nanoclay paste, so the crossover of the $G'$ and $G''$ curves occurs at a higher $\omega$ of 50 rad/s. This suggests that the stress relaxation lessening is less severe for the fumed alumina paste than for the nanoclay paste, i.e., the stress relaxation is faster for the fumed alumina paste. The slow stress relaxation for the nanoclay paste is probably due to the nanoplatelet morphology and the relative difficulty of movement of one nanoplatelet with respect to another. In contrast, the fast stress relaxation for the fumed alumina paste is probably due to the aggregate morphology and the relative ease of movement of one aggregate with respect to another.

For both CB(Cabot) paste (Fig. 7c) and CB(Tokai) paste (Fig. 7d), $G'$ exceeds $G''$ for all $\omega$ values. This means that these pastes are solid-like at all frequencies studied.[27,29] For the CB(Cabot) paste, $G''$ increases and approaches $G'$ as $\omega$ increases, meaning that the paste becomes more and more liquid-like as $\omega$ increases, though it remains mainly solid-like. In contrast, the CB(Tokai) paste remains similar in its high degree of solid-like character at all frequencies, with $G'$ and $G''$ not changing much as $\omega$ increases, due to its high solid content. For the CB(Tokai) paste, $G''$ decreases slightly and $G'$ increases slightly with increasing $\omega$ in the range below 3 rad/s, probably because of the small extent of stress relaxation at all frequencies in this solid-like material and the reduction of the contribution of viscous deformation to the overall deformation as $\omega$ increases, as explained in the "Background on Rheology" section.

Table VI lists the values of $G'$, $G''$, and $|\eta|$ at 0.1 rad/s and 100 rad/s. At both angular frequencies, the $G'$ and $G''$ values are low for the nanoclay paste, higher for the fumed alumina paste, significantly higher for the CB(Cabot) paste, and much higher for the CB(Tokai) paste. At 100 rad/s, tan $\delta$ is highest for the nanoclay paste and lowest for the CB(Tokai) paste, as in Table II, which is for an angular frequency of 6.28 rad/s (1 Hz). However, at 1 rad/s, tan $\delta$ is lowest for the nanoclay paste and highest for the fumed alumina paste. This behavior relates to the fact that tan $\delta$ increases with increasing frequency for the nanoclay paste, the fumed alumina paste, and the CB(Cabot) paste, but it decreases with increasing frequency for the CB(Tokai) paste, as shown in Fig. 7e.

The effect of frequency on tan $\delta$ is mainly due a similar effect of frequency on $G''$. This means that the increase in tan $\delta$ without increasing frequency, as observed for the nanoclay paste over the entire frequency range and for the fumed alumina paste and the CB(Cabot) paste in the high-frequency regime, is due to increase in $G''$, i.e., increase in the fluid-like character. Similarly, the decrease in tan $\delta$ without increasing frequency, as observed for the CB(Tokai) paste in the low-frequency regime, is due to decrease in $G''$, i.e., decrease in the fluid-like character. The decrease in $G''$ with increasing frequency is attributed to the increasing inadequacy in time for viscous deformation to occur as the frequency increases. This inadequacy is particularly severe when the material is solid-like, as in the case of the CB(Tokai) paste.

A similar frequency sweep conducted by Feger et al.[24] shows results that are somewhat similar to those of the CB(Tokai) paste, with $G'$ higher than $G''$ over the entire frequency range and the viscosity decreasing with increasing frequency. However, due the high volume fraction of the solid component, the $G'$, $G''$, and viscosity reported by Feger et al. are much higher than those of all the pastes studied here, as shown in Table VI.

Figure 8 shows that, for the vehicle in the absence of a solid component, $G'$ exceeds $G''$ at all angular frequencies investigated, whether antioxidants are present or not. This means that the vehicle is fluid-like, whether antioxidants are present or not. This behavior is in contrast to the mainly solid-like

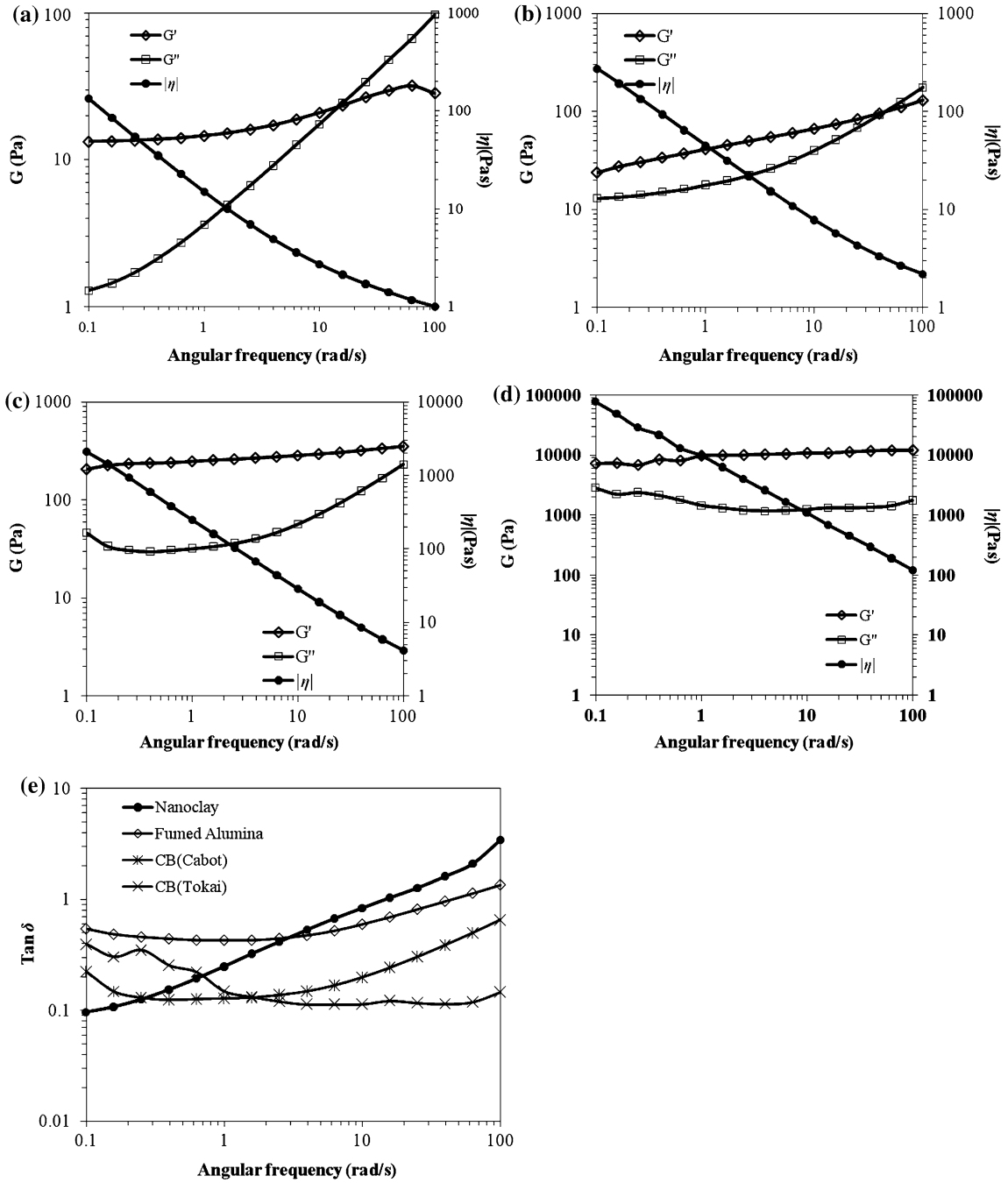


Fig. 7. Effect of the angular frequency $\omega$ on the storage modulus $G'$, loss modulus $G''$, complex apparent viscosity magnitude $|\eta|$, and tan $\delta$ for: (a) the nanoclay paste, (b) the fumed alumina paste, (c) the CB(Cabot) paste, and (d) the CB(Tokai) paste. (e) The tan $\delta$ of various thermal pastes.

character when a solid component (any of those studied) is present (Fig. 7). Even for the nanoclay, which is used at only 1 vol.%, its presence changes the behavior from fluid-like behavior to solid-like behavior.

Figure 8 shows that the addition of the antioxidants to the vehicle in the absence of a solid component increases $G'$ significantly, increases $G''$ negligibly, and increases $|\eta|$ (apparent viscosity) for all angular frequencies studied. This suggests that, without a solid component, the antioxidants mainly affect the elastic properties, while the viscous properties are not affected. The increase in $|\eta|$ is consistent with a prior report.[22] As $\omega$ increases, $|\eta|$ does not change, whether antioxidants are present or not. This means that the viscosity is independent of the shear rate, i.e., the vehicle is Newtonian. As $\omega$ increases, both $G'$ and $G''$ increase, whether

**Table VI. Comparison of the Values of $G'$, $G''$, $|\eta|$ (Apparent Viscosity), and tan $\delta$ at Angular Frequencies of 0.1 rad/s and 100 rad/s for Various Thermal Pastes**

| | 0.1 rad/s | | | | 100 rad/s | | | |
|---|---|---|---|---|---|---|---|---|
| **Paste** | $G'$ (Pa) | $G''$ (Pa) | $\|\eta\|$ (Pa s) | tan $\delta$ | $G'$ (Pa) | $G''$ (Pa) | $\|\eta\|$ (Pa s) | tan $\delta$ |
| Nanoclay | 13.4 | 1.29 | 134 | 0.10 | 28.5 | 97.0 | 1.01 | 3.40 |
| Fumed alumina | 23.9 | 13.0 | 272 | 0.55 | 130 | 176 | 2.18 | 1.35 |
| CB(Cabot) | 205 | 45.9 | 2105 | 0.22 | 352 | 230 | 4.21 | 0.65 |
| CB(Tokai) | 7279 | 287 | 78250 | 0.39 | 12160 | 1779 | 123 | 0.15 |
| Ref. 24 | $\sim 3.3 \times 10^5$ | $\sim 1.8 \times 10^5$ | $\sim 3.7 \times 10^5$ | $\sim$0.55 | $\sim 3.5 \times 10^3$ | $\sim$900 | $\sim 3.5 \times 10^3$ | $\sim$0.26 |

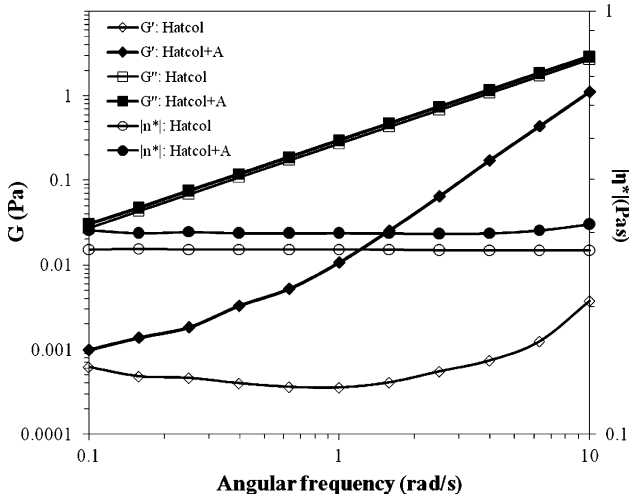


Fig. 8. Effect of the angular frequency $\omega$ on the storage modulus $G'$, loss modulus $G''$, and complex viscosity magnitude $|\eta|$ for the vehicle without solid, showing comparison of the vehicle with and without antioxidants. A = antioxidants.

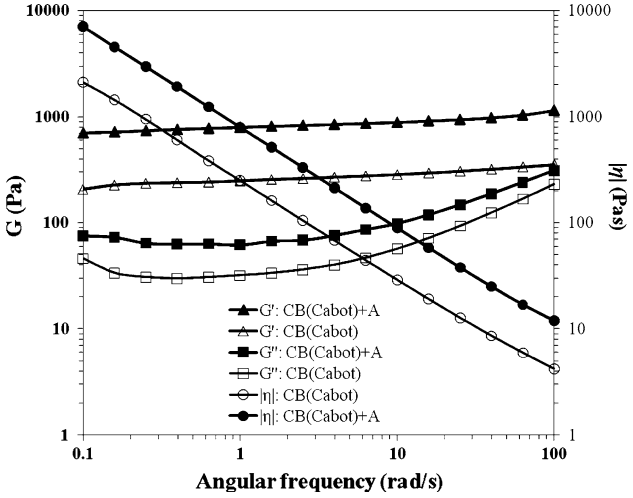


Fig. 9. Effect of the angular frequency $\omega$ on the storage modulus $G'$, loss modulus $G''$, and complex viscosity magnitude $|\eta|$, showing comparison of the CB(Cabot) pastes with and without antioxidants. A = antioxidants.

antioxidants are present or not, except that, in the absence of antioxidants, $G'$ decreases slightly with increasing $\omega$ from 0.1 rad/s to 1 rad/s. The increase of $G'$ and $G''$ is attributed to the lessening stress relaxation as $\omega$ increases. The origin of the slight decrease of $G'$ with increasing $\omega$ from 0.1 rad/s to 1 rad/s is presently not clear.

Comparison of Fig. 8 (case without antioxidants) with Fig. 7 in relation to the viscosity shows that the addition of a solid component causes the change from Newtonian behavior to shear-thinning behavior. Comparison in relation to $G''$ shows that the increase in $G''$ with increasing $\omega$ for the nanoclay paste, the fumed alumina paste, and the CB(Cabot) paste stems from the similar increase for the vehicle itself. That $G''$ varies little with $\omega$ for the CB(Tokai) paste (Fig. 7d) is in contrast to the increase of $G''$ with increasing $\omega$ for the vehicle alone (Fig. 8). This difference is attributed to the strong solid-like character of the CB(Tokai) paste.

Figure 9 shows that, for the CB(Cabot) paste, $G'$, $G''$, and $|\eta|$ are all increased by the addition of antioxidants, such that the frequency dependence is not affected. The increases in $G'$ and $|\eta|$ upon addition of antioxidants are consistent with the increases of these parameters upon addition of antioxidants in the absence of a solid component (Fig. 8). The increase in $G''$ (Fig. 9) is in contrast to the negligible increase upon addition of antioxidants in the absence of a solid component (Fig. 8). This suggests that the antioxidants have a strong interaction with the carbon black, since the presence of the antioxidants significantly increases $G'$, which relates to the network of carbon black. The effect of antioxidants on $G'$, $G''$, and viscosity of the vehicle and the pastes at room temperature has not been previously reported.[22]

Figure 10 shows that, for the CB(Cabot) paste, tan $\delta$ is decreased by the addition of antioxidants, such that the frequency dependence is essentially not affected. This means that the addition of antioxidants promotes solid-like behavior. Whether antioxidants are present or not, tan $\delta$ decreases slightly upon increasing $\omega$ from 0.1 rad/s to 1 rad/s and increases significantly upon increasing $\omega$ from 1 rad/s to 100 rad/s. The slight decrease in tan $\delta$ with increasing $\omega$ from 0.1 rad/s to 1 rad/s is probably due to viscous deformation having less time to

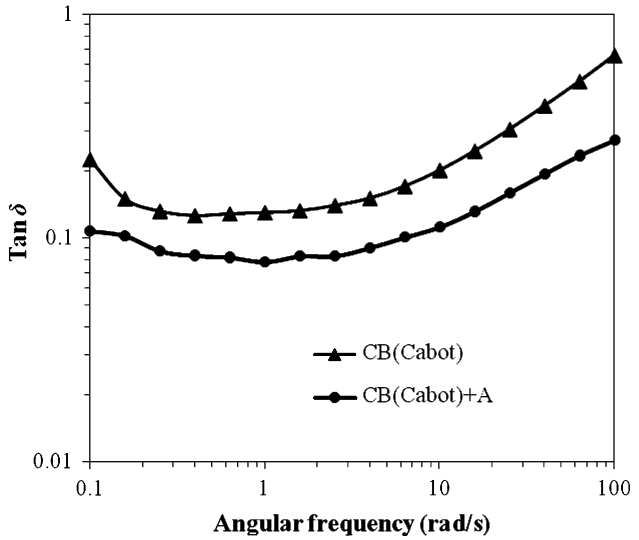


Fig. 10. Effect of the angular frequency $\omega$ on tan $\delta$, showing comparison of the CB(Cabot) pastes with and without antioxidants. A = antioxidants.

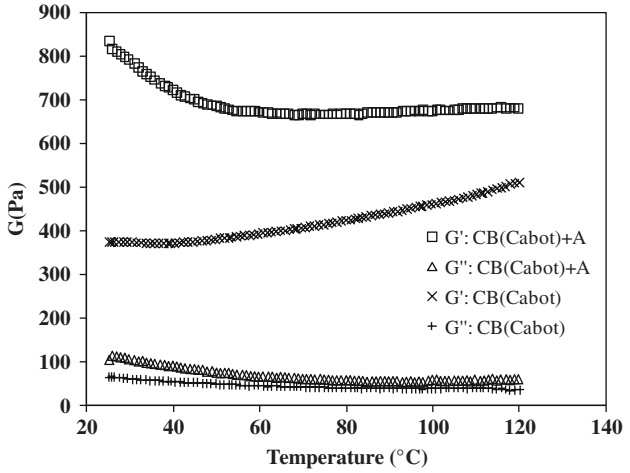


Fig. 11. Effect of increasing temperature on the storage modulus $G'$ and loss modulus $G''$ of the CB(Cabot) paste with and without antioxidants. A = antioxidants.

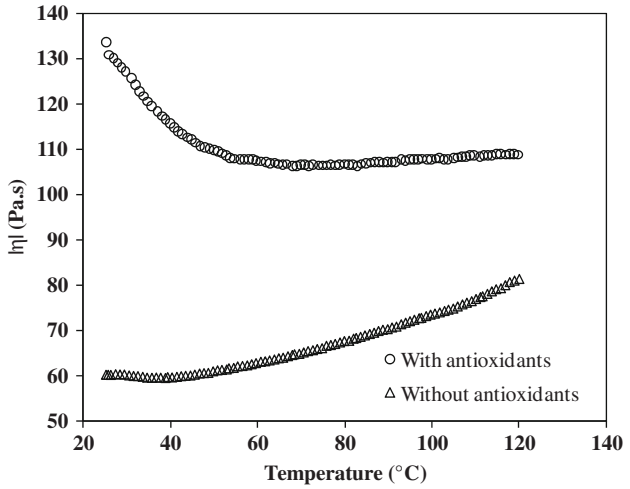


Fig. 12. Effect of increasing temperature on the complex apparent viscosity magnitude $|\eta|$ for the CB(Cabot) paste with and without antioxidants.

occur as $\omega$ increases. The increase in tan $\delta$ with increasing $\omega$ from 1 rad/s to 100 rad/s is probably due to a certain stress relaxation mechanism not having enough time to operate sufficiently as $\omega$ increases. At all frequencies studied, tan $\delta$ is less than 1, thus supporting a solid-like character,[27,29] whether antioxidants are present or not.

## Effect of Increasing Temperature

Figure 11 shows that, for the CB(Cabot) paste in the absence of antioxidants, increasing temperature from 25°C to 120°C increases $G'$ slightly and decreases $G''$ very slightly. This effect is due to slight phase separation (as indicated by visual observation of a small amount of vehicle seeping out of the specimen as the temperature was increased during the rheological testing) and consequent effective increase of the solid volume fraction of the paste and hence enhancement of the solid-like character.

In the presence of antioxidants, $G'$ decreases as the temperature increases from 25°C to 50°C, followed by negligible change as the temperature increases beyond 50°C, while $G''$ decreases slightly as the temperature increases from 25°C to 60°C, followed by negligible change as the temperature increases beyond 60°C (Fig. 11). These effects in the presence of antioxidants are probably because heating below 60°C increases the fluidity of the paste and heating above 60°C reveals the thermal stabilization effect of the antioxidants.

The effect of heating on the rheology of thermal pastes is in contrast to that of filled polymer systems,[33] which typically soften (becoming more fluid-like) upon heating, so that $G'$ decreases and $G''$ increases. This difference stems from the high thermal stability of polymers compared with the vehicle used in a thermal paste.

Figure 12 shows that, for the CB(Cabot) paste, the addition of antioxidants increases the apparent viscosity at all temperatures studied. In the absence of antioxidants, the viscosity increases with increasing temperature from 25°C to 120°C, probably due to slight phase separation, slight evaporation of the vehicle, and/or occurrence of crosslinking during heating.[22] However, in the presence of antioxidants, the viscosity decreases as the temperature increases from 25°C to 50°C and remains essentially unchanged as the temperature further increases from 50°C to 120°C. These effects in the presence of antioxidants are probably because heating below 50°C increases the fluidity of the paste and heating above 50°C reveals the thermal stabilization effect of the antioxidants.

It is important to note that this test was conducted at a gap distance of 1 mm, which is more than a thousand times larger than the submicron bond-line thickness of thermal pastes.[20] Thus, in practical situations, phase separation is expected to be much less severe than the slight separation observed during rheological testing.

Feger et al.[24] conducted rheological measurement of hydrocarbon-oil-based thermal pastes containing more than 72 vol.% of a mixture of alumina and aluminum particles during heating from 25°C to 100°C and found that $G'$, $G''$, and $|\eta|$ all decreased significantly with increasing temperature, with $G'$ decreasing by 99%, $G''$ decreasing by 98%, and $|\eta|$ decreasing by 99.9%. In contrast, in this work, for the CB(Cabot) paste without antioxidants, $G'$ increased by only 37%, $G''$ decreased by only 77%, and $|\eta|$ increased by only 74%. For the CB(Cabot) paste with antioxidants, $G'$ decreased by only 22%, $G''$ decreased by only 73%, and $|\eta|$ decreased by only 23%. Thus, whether antioxidants are present or not, the CB(Cabot) paste is much more thermally stable than the paste of Feger et al.

The effect of prior heating on the room-temperature viscosity (as measured by using a viscometer) of the polyol ester vehicle without a solid component has been previously reported by Aoyagi and Chung.[22] In the absence of antioxidants, the viscosity of the vehicle increases significantly after heating at 200°C for times as short as 2 h. In the presence of antioxidants, the viscosity essentially does not change, even after heating at 200°C for 48 h. The increase in viscosity in the absence of antioxidants suggests the occurrence of crosslinking during heating. However, the viscosity change in the presence of a solid component was not reported and the change of the viscosity during heating was not investigated.

## Relationship of Thermal Performance and Rheological Behavior of Thermal Pastes

The performance of a thermal paste is indicated by the thermal contact conductance of the sandwich comprising the thermal paste and the two proximate surfaces sandwiching it. Table VII presents the values of the thermal contact conductance, as measured using the guarded hot-plate method by sandwiching the paste between two copper surfaces of controlled roughness (either 15 $\mu$m or 0.01 $\mu$m), with a controlled pressure (0.46 MPa, 0.69 MPa or 0.92 MPa) applied perpendicular to the thermal interface. Refer to Ref. 19 for details of the method.

Among the various solid components, nanoclay at 1.0 vol.% gives the lowest $G'$ and $G''$ and the highest $\gamma_c$ and tan $\delta$ (Table II). This is consistent with a low bond-line thickness[20] and the highest thermal contact conductance for the case of smooth proximate surfaces (Table VII). The contact conductance is high in spite of the low thermal conductivity (Table VII), because of the relatively strong

**Table VII. Thermal Contact Conductance of Various Thermal Pastes. Each Paste Is Sandwiched by Two Copper Surfaces of Controlled Roughness (15 $\mu$m or 0.009 $\mu$m), with a Controlled Pressure (0.46 MPa, 0.69 MPa or 0.92 MPa) Applied Perpendicular to the Thermal Interface**

| | | Thermal Contact Conductance ($10^4$ W/m$^2$ K) | | | | | | | |
|---|---|---|---|---|---|---|---|---|---|
| | | Rough Surfaces (15 $\mu$m) | | | Smooth Surfaces (0.009 $\mu$m) | | | | |
| Paste | Solid Component, vol.% | 0.46 MPa | 0.69 MPa | 0.92 MPa | 0.46 MPa | 0.69 MPa | Bond-Line Thickness[a] ($\mu$m) | Thermal Conductivity (W/m K) |
| Vehicle[20] | 0.0 | 10.50 ± 0.60 | 10.70 ± 0.10 | 11.30 ± 0.20 | 28.79 ± 0.16 | 32.72 ± 1.62 | 0.21 ± 0.01 | 0.119 |
| Vehicle + A[22] | 0.0 | 11.00 ± 0.10 | 11.00 ± 0.10 | 11.90 ± 0.20 | – | – | – | – |
| Nanoclay paste[20] | 1.0 | 7.87 ± 0.05 | 8.50 ± 0.25 | 8.95 ± 0.10 | 30.66 ± 1.69 | 39.30 ± 1.60 | 0.22 ± 0.01 | 0.120 |
| Fumed alumina paste[19,20] | 2.4 | 10.00 ± 0.24 | 10.55 ± 0.28 | 10.52 ± 0.27 | 25.13 ± 0.76 | 27.76 ± 0.25 | 0.22 ± 0.01 | 0.123 |
| CB(Cabot) paste[16,18] | 2.4 | 9.70 ± 0.11 | 10.23 ± 0.11 | 11.79 ± 0.27 | 25.91 ± 0.16 | 27.75 ± 0.14 | 0.22 ± 0.00 | 0.128 |
| CB(Cabot) paste + A [this work] | 2.4 | 8.89 ± 0.10 | 9.29 ± 0.10 | 9.65 ± 0.21 | 22.67 ± 0.41 | 25.42 ± 0.12 | 0.23 ± 0.01 | 0.125 |
| CB(Tokai) paste[16,18] | 8.0 | 11.27 ± 0.34 | 12.41 ± 0.22 | 13.18 ± 0.11 | 25.58 ± 0.35 | 27.86 ± 0.10 | 0.27 ± 0.02 | 0.225 |

A = Antioxidants. The testing methods for all the pastes are identical. [a]Measured for the case of smooth (0.009 $\mu$m) copper surfaces.

fluid-like character, which is particularly important for the case of smooth surfaces. The undulations on a smooth surface are more microscopic than those on a rough surface.

The CB(Tokai) at 8 vol.% gives the highest $G'$ and $G''$ and the lowest $\gamma_c$ and tan $\delta$ (Table II). This is consistent with the highest bond-line thickness.[18] However, due to the high CB(Tokai) volume fraction, the thermal conductivity is the highest,[20] thus resulting in the highest thermal contact conductance for the case of rough proximate surfaces (Table VII).

Fumed alumina at 2.4 vol.% gives lower $G'$ and $G''$ and higher $\gamma_c$ and tan $\delta$ than CB(Cabot) that is also at 2.4 vol.% (Table II). In other words, the fumed alumina paste is more fluid-like than the CB(Cabot) paste. However, fumed alumina and CB(Cabot) give similar values of the bond-line thickness[19,35] and hence similar values of the thermal contact conductance for both rough and smooth cases (Table VII). The similarity in bond-line thickness may be due to the high error of the small bond-line thickness values measured. The similarity in thermal contact conductance may be due to the complexity of factors that govern the conductance.[36]

The vehicle in the absence of a solid component gives high values of the thermal contact conductance (Table VII), due to its fluid-like character and expected low bond-line thickness. However, it is not suitable for use as a TIM, due to the high tendency for it to seep out of the thermal interface.

The presence of the antioxidants decreases the thermal contact conductance, as shown in Table VII by comparing the CB(Cabot) paste with and without antioxidants. This is due to a slightly higher bond-line thickness and a lower thermal conductivity when the antioxidants are present. The higher bond-line thickness is due to the increased mechanical rigidity of the thermal paste, as supported by the higher apparent viscosity, yield stress, and $G'$. The lower thermal conductivity is probably because the antioxidants interact with the carbon black surface,[22] thereby affecting the thermal resistance of the interface between adjacent carbon particles.

Since there are numerous factors that govern the performance of a thermal paste,[36] such as thermal conductivity, bond-line thickness, conformability, spreadability, and surface roughness, it is difficult to arrive at a general relation between the thermal contact conductance and the rheological parameters of thermal pastes. Nevertheless, the effect of antioxidants on the rheology and the thermal contact conductance of the CB(Cabot) paste shows a clear relationship. The addition of antioxidants decreases the thermal contact conductance for both smooth and rough surfaces (Table VII), while it increases $G'$, the yield stress, and the viscosity (Table VI) (i.e., it increases the mechanical rigidity). Greater rigidity is expected to increase the bond-line thickness, thereby lowering the thermal contact conductance.[23]

The bond-line thickness is one of the dominant factors that affect the performance of high-performance thermal pastes. It is directly related to the yield stress of the pastes and the applied pressure.[16,23] The high conformability, as enabled by the nanosized and squishable filler, and the high spreadability, as enabled by the low viscosity, result in a low bond-line thickness.

## CONCLUSIONS

The rheological behavior of thermal pastes with a polyol-ester-based vehicle (with and without dissolved antioxidants) and 1.0 vol.% to 8.0 vol.% nanoscale solid [nanoclay, fumed alumina, CB(Cabot) and CB(Tokai)] have been studied. All the pastes exhibit Bingham plastic behavior with shear thinning. Double yielding occurs in the CB(Cabot) and CB(Tokai) pastes but not in the nanoclay and fumed alumina pastes. The plastic viscosity after complete yielding is higher when the solid volume fraction is higher. The antioxidants cause the plastic viscosity and the first and second yield stresses to be higher.

In the absence of a solid component, the vehicle is Newtonian and fluid-like, with $G''$ higher than $G'$. In the presence of any of the solid components, the paste is shear thinning and is mainly solid-like, with $G'$ higher than $G''$. The addition of antioxidants increases all of $G'$, $G''$, and the viscosity and decreases tan $\delta$ and the critical strain $\gamma_c$, hence enhancing the solid-like character and decreasing the thermal contact conductance, which indicates the thermal paste performance. The value of tan $\delta$ is below 1, such that it is frequency dependent. In the case of CB(Cabot) at 2.4 vol.%, tan $\delta$ increases with increasing angular frequency from 1 rad/s to 100 rad/s.

Among the various solid components, nanoclay at 1.0 vol.% gives the lowest $G'$ and $G''$ and the highest $\gamma_c$ and tan $\delta$,, thus resulting in a low bond-line thickness and the highest thermal paste performance for smooth proximate surfaces. The CB(Tokai) at 8.0 vol.%, due to the high solid volume fraction, gives the highest $G'$ and $G''$ and the lowest $\gamma_c$ and tan $\delta$, thus resulting in the highest bond-line thickness, though the high thermal conductivity due to the high solid volume fraction results in the highest thermal paste performance for rough proximate surfaces.

In the absence of antioxidants, $G'$ and the apparent viscosity increase upon heating from 25°C to 120°C, while $G''$ decreases, due to slight phase separation. The antioxidants improve the ability to withstand temperatures up to 120°C by reducing the tendency for phase separation at elevated temperature, so that $G'$, $G''$, and the apparent viscosity do not change upon heating from 50°C to 120°C. In the presence of antioxidants, $G'$, $G''$, and the apparent viscosity decrease upon heating from 25°C to 50°C, due to increase in fluidity.

## ACKNOWLEDGEMENTS

Special thanks go to Dr. Terri Chen and Dr. Madhu Namani of TA Instruments—Waters LLC (New Castle, DE) for the rheological testing service.

## REFERENCES

1. E.G. Wolff and D.A. Schneider, *Int. J. Heat Mass Transf.* 41, 3469 (1998).
2. T. Ouellette and M. Sorgo, *Proceedings of the Power Electronics Design Conference, Power Sources Users Conference*, Cerritos, CA (1985), pp. 134–138.
3. M.R. Vogel, *Proceedings of the International Intersociety of Electronic Packaging Conference, Advances in Electronic Packaging*, vol. 10–2 (American Society of Mechanical Engineers, 1995), p. 989.
4. V. Sartre and M. Lallemand, *Appl. Therm. Eng.* 21, 221 (2001).
5. M. Grujicic, C.L. Zhao, and E.C. Dusel, *Appl. Surf. Sci.* 246, 290 (2005).
6. D.D.L. Chung, *J. Mater. Eng. Perform.* 10, 56 (2001).
7. N.G. Aakalu and L.A. Rittmiller, U.S. patent 4,265,775 (5 May 1981).
8. R. Anderson and R.B. Booth, *IEEE Trans. Component. Hybrid. Manuf. Technol.* 13, 713 (1990).
9. S. Iruvanti, R.K. Gupta, and E. Ruckenstein, U.S. patent 5,098,609 (24 March 1992).
10. S. Iruvanti, K.S. Olsen, and K.G. Sachdev, U.S. patent 5,591,789 (7 January 1997).
11. Y. Xu, X. Luo, and D.D.L. Chung, *J. Electron. Packag.* 124, 188 (2002).
12. C.-K. Leong and D.D.L. Chung, *Carbon* 41, 2459 (2003).
13. C.-K. Leong and D.D.L. Chung, *Carbon* 42, 2323 (2004).
14. C.-K. Leong, Y. Aoyagi, and D.D.L. Chung, *J. Electron. Mater.* 34, 1336 (2005).
15. C.-K. Leong, Y. Aoyagi, and D.D.L. Chung, *Carbon* 44, 435 (2006).
16. C. Lin and D.D.L. Chung, *Carbon* 45, 2922 (2007).
17. A. Yu, P. Ramesh, M.E. Itkis, E. Bekyarova, and R.C. Haddon, *J. Phys. Chem. C* 111, 7565 (2007).
18. C. Lin and D.D.L. Chung, *Carbon* 47, 295 (2009).
19. C. Lin and D.D.L. Chung, *J. Mater. Sci.* 42, 9245 (2007).
20. C. Lin and D.D.L. Chung, *J. Electron. Mater.* 37, 1698 (2008).
21. C. Lin, T.A. Howe, and D.D.L. Chung, *J. Electron. Mater.* 36, 659 (2007).
22. Y. Aoyagi and D.D.L. Chung, *J. Mater. Sci.* 42, 2358 (2007).
23. R. Prasher, J. Shipley, S. Prstic, P. Koning, and J.-L. Wang, *ASME, Heat Transfer Div. HTD* 372, 47 (2002).
24. C. Feger, J.D. Gelorme, M. McGlashan-Powell, and D.M. Kalyon, *J. Res. Dev.* 49, 699 (2005).
25. C.L. Barrie, P.C. Griffiths, R.J. Abbott, I. Grillo, D. Kudryashov, and C. Smyth, *J. Colloid Interface Sci.* 272, 210 (2004).
26. C.W. Macosko, *Rheology Principles, Measurements and Applications* (USA: Wiley-VCH, 1994).
27. A.J. Franck, Application of Rheology of Polymers, TA Instruments, http://www.tainstruments.com/library_download.aspx?file=AAN016_V1_U_StructFluids.pdf, as on May, 2009.
28. S. Aoshima, *Wax Crystal Control—Nanocomposites—Stimuli-Responsive Polymers (Advances in Polymer Science)* (Springer, Berlin, 2007).
29. Y. Lee, B. Chae, A. Lane, and J. Wiest, *Colloids Surf. A Physicochem. Eng. Asp.* 224, 23 (2003).
30. P. Herh, J. Tkachuk, S. Wu, M. Bernzen, and B. Rudolph, *Am. Lab.* July, 12 (1998).
31. N.P. Cheremisinoff, *Polymer Mixing and Extrusion Technology*, 1st ed. (Boca Raton, FL: CRC, 1987), p. 77.
32. J.C. Salamone, *Polymeric Materials Encyclopedia*, 1st ed. (Boca Raton, FL: CRC, 1996), p. 6616.
33. A.V. Shenoy, *Rheology of Filled Polymer Systems* (Norwell, MA: Kluwer Academic, 1999), p. 80.
34. Y. Zhong and S. Wang, *J. Rheol.* 47, 483 (2003).
35. C. Lin and D.D.L. Chung, *Nanostructured Thermal Interface Pastes for Microelectronic Cooling Proc. Fall Technical Conference* (SAMPE, Memphis, TN, Sept. 2008).
36. P. Pour Shahid Saeed Abadi, C.-K. Leong, and D.D.L. Chung, *Electron. Mater.* 38, 175 (2009).